A Large-scale Neural Model Inversion Framework for Effective Connectivity Estimation

Guoshi Li[0000−0002−8984−4722] and Pew-Thian Yap[0000−0003−1489−2102]

Department of Radiology and Biomedical Research Imaging Center (BRIC), University of North Carolina at Chapel Hill, Chapel Hill, USA
ptyap@med.unc.edu

Abstract. The development of a computational framework that can infer large-scale brain-wide effective connectivity (EC) based on resting-state functional MRI (rs-fMRI) represents a grand challenge to computational neuroimaging. Towards the goal of estimating full-scale, whole-brain EC, we developed a new computational framework termed Large-scale nEural Model Inversion (LEMI) by utilizing a linear neural mass model with an efficient Kalman-filter based gradient descent algorithm. Key advantages of LEMI include fast estimation of both intra-regional and inter-regional connection strengths for large-scale networks, allowing exploration of both intrinsic and external mechanisms in neuroscience problems. Using ground-truth simulations, we demonstrated that LEMI can accurately and efficiently recover model parameters in a large network (100 regions) within 90 minutes. We then applied the LEMI model to an empirical rs-fMRI dataset from the ADNI database and identified widespread reduced excitation-inhibition (E-I) ratio in patients with Alzheimer's disease (AD). Overall, LEMI provides an efficient and accurate computational framework to estimate large-scale EC and whole-brain E-I balance based on non-invasive neuroimaging data.

Keywords: Neural Mass Model · Effective Connectivity · Optimization.

1 Introduction

The advancement of non-invasive neuroimaging techniques, such as functional magnetic resonance imaging (fMRI), has enabled the development of sophisticated tools and models to elucidate the organizational principles of the human brain at an extraordinary level of detail. Computational connectomics has played a particularly important role in mapping the functional architecture of large-scale brain networks in health and potential alterations in diseases [4,25]. There are two major types of analysis approaches in the field of fMRI connectome including functional connectivity (FC) and effective connectivity (EC) [12]. FC represents the statistical dependency among fMRI signals which can be either undirected or directed [11]. While undirected FC can be computed using simple correlation analyses (e.g., Pearson's correlation), directed FC is usually computed by more sophisticated statistical approaches such as Granger causality [11]. Despite the widespread use and great success of FC in characterizing the functional organization of large brain-wide networks in both task and resting-state conditions, its clinical application is still limited in that it does not offers a neurophysiological account

of the aberrant neural process in diseases. Effective connectivity, in contrast, characterizes the directed causal influence among neuronal populations with biologically plausible neuronal models [9,11], thus able to offer neural-based mechanistic account of cognitive function and dysfunction [26].

However, estimating EC in large-scale brain networks is highly challenging due to complex computation (e.g., integration of differential equations and nonlinear optimization). As a predominant method to compute EC, dynamic causal modeling (DCM) is restricted to relatively small networks (usually on the order of 10 regions) [9], though two new variants of DCM (spectral DCM and regression DCM) have potential for brain-wide application [13,21]. In addition, DCM-based models for fMRI primarily use simple one-state model for generating neural activity, which restricts their biological relevance. Though the latest DCM incorporates a hierarchical neural mass model (NMM) of neuronal dynamics, it is currently applied to task-based fMRI only [10].

Two recent developments in EC models precisely address the limitations of DCM. The first framework, termed Multiscale Neural Model Inversion (MNMI), aims to connect mesoscale circuit interactions with macroscale network connectivity and identify both intra-regional and inter-regional EC based on resting-state fMRI (rs-fMRI) [18,19]. The biological realism and model flexibility make MNMI an attractive framework to estimate EC in biophysical networks. However, the size of the MNMI model is designed to be relatively small (< 50 brain regions) due to heavy computational burden, whereas neuropsychiatric disorders typically involve much larger networks [4,20]. Concurrently, Singh et al. [24] developed a new modeling approach termed Mesoscale Individualized Neurodynamic (MINDy) modeling which fits nonlinear dynamical systems models directly to rs-fMRI data. Notably, the MINDy framework is able to estimate data-driven network models with hundreds of interacting brain regions in just a few minutes per subject, making it ideal for large-scale network construction and big dataset application. Nevertheless, the model includes only one neural population per region and thus cannot model intra-regional neural interactions.

In this study, we attempt to combine the advantages of MNMI and MINDy and develop an accurate and efficient computational framework for EC estimation. We term this new framework Large-scale nEural Model Inversion (LEMI). Simulation shows that LEMI can accurately estimate local recurrent excitation and inhibition strengths as well as inter-regional EC in large-scale networks (up to 100 regions) in just tens of minutes on a standard computer. After validation, we applied the LEMI model to the Alzheimer's Disease Neuroimaging Initiative (ADNI) dataset and identified large-scale E-I imbalance in both mild cognitive impairment (MCI) and AD patients. Overall, the LEMI framework holds the promise to estimate large-scale EC and E-I balance for the identification of potential biomarkers and pathophysiological mechanisms in neurological and psychiatric disorders.

2 Methods

2.1 Overview of the LEMI Framework

In the LEMI framework (Fig. 1A), each network node contains two mutually coupled excitatory (E) and inhibitory (I) neural populations. The E neural population excites

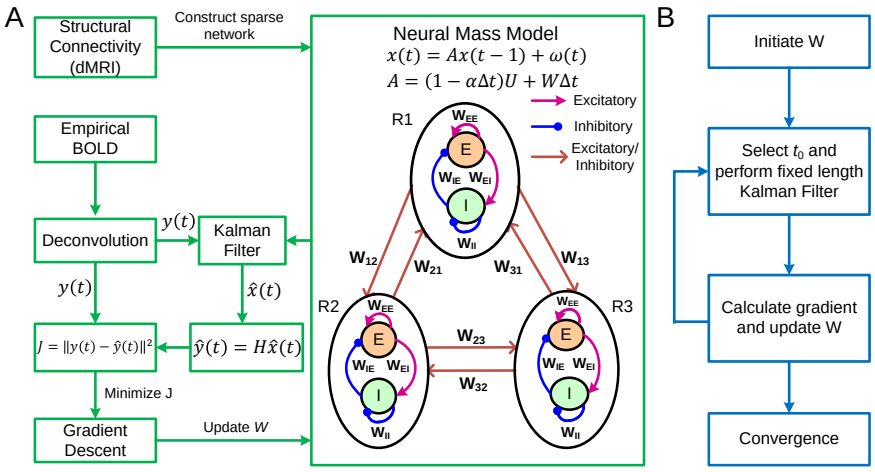

Fig. 1. Overview of the LEMI framework. (A) LEMI diagram. (B) Optimization algorithm.

the I neural population while receiving feedback inhibition from the latter. The E neural population receives self-excitation and long-range inputs from other brain regions. First, structural connectivity from diffusion MRI (dMRI) is used to construct a sparse network by removing weak connections. Second, empirical blood-oxygen-level-dependent (BOLD) signals are Wiener-deconvolved [24] to obtain composite neural activity $y(t)$; we choose Wiener Deconvolution due to its optimal noise reduction and signal restoration [28]. Third, Kalman filter is applied to estimate neural activity $x(t)$ [23] and the predicted error of the composite neural activity is calculated. Lastly, gradient descent algorithm is used to optimize model parameters by minimizing the prediction error.

2.2 The Neural Mass Model

The neural network dynamics are described by a discrete linearized NMM of Wilson-Cowan type [14,29]:

$$x(t) = Ax(t-1) + \omega(t), \tag{1}$$

$$y(t) = Hx(t) + v(t), \tag{2}$$

$$x = \begin{bmatrix} \mathrm{E} \\ \mathrm{I} \end{bmatrix}, W = \begin{bmatrix} W_{\mathrm{RE}} & W_{\mathrm{IE}} \\ W_{\mathrm{EI}} & W_{\mathrm{II}} \end{bmatrix}, A = (1 - \alpha\Delta t)U + W\Delta t, \tag{3}$$

where E and I are the mean neural activity in the vector form (M $\times$ 1), Δt is the sampling TR, α is the decay rate, U is an identity matrix, H is the observation matrix which maps the neural activity into the deconvolved BOLD, $y(t)$ is the composite neural activity (i.e., deconvolved BOLD) ($y = 2/3\mathrm{E} + 1/3\mathrm{I}$, [19]), and $\omega(t)$ and $v(t)$are Gaussian white noise. W_{RE} encodes interactions among E neural populations ($W_{\mathrm{RE}} = W_{\mathrm{RR}} + W_{\mathrm{EE}}$) where W_{RR} is the inter-regional EC (with zero diagonal), and W_{EE}, W_{EI}, W_{IE} and W_{II} are diagonal matrices (M $\times$ M) representing the local E $\rightarrow$ E, E $\rightarrow$ I, I $\rightarrow$ E and I $\rightarrow$ I connection strengths, respectively.

2.3 Estimation of Neural Activity

The neural activity $x(t)$ is estimated using Kalman filter based on the deconvolved BOLD signal $y(t)$ (Fig. 1A). Assuming $\omega(t) \sim \mathcal{N}(0, Q)$ and $v(t) \sim \mathcal{N}(0, R)$, the estimation process is formulated as [17]:

Prediction:

$$\hat{x}_{t|t-1} = A\hat{x}_{t-1} \tag{4}$$

$$P_{t|t-1} = AP_{t-1}A^T + Q \tag{5}$$

Update:

$$K_k = P_{t|t-1}H^T(HP_{t|t-1}H^T + R)^{-1} \tag{6}$$

$$\hat{x}_t = \hat{x}_{t|t-1} + K_k(y(t) - H\hat{x}_{t|t-1}) \tag{7}$$

$$P_t = (I - K_kH)P_{t|t-1} \tag{8}$$

2.4 Estimation of Neural Model Parameters

Connection parameters (W) are optimized by minimizing the following cost function:

$$J = \frac{1}{L}\sum_{t=t_0}^{t_0+L}\sum_{k=1}^{M}(y_k(t) - \hat{y}_k(t))^2 \tag{9}$$

where L is the number of samples in a randomly selected time segment, M is the number of regions, and $\hat{y}(t)$ is the estimate of $y(t)$ ($\hat{y}(t) = H\hat{x}(t)$). The cost function is minimized using Nesterov-Accelerated Adaptive Moment Estimation (NADAM, [6]), a stochastic gradient-descent algorithm with fast convergence and over-fitting prevention. The NADAM algorithm iteratively updates parameters as follows [24]:

$$m_{k+1} = \mu m_k + (1-\mu)\frac{\partial J}{\partial W_k}, \quad n_{k+1} = \nu n_k + (1-\nu)\frac{\partial J^2}{\partial W_k} \tag{10}$$

$$W_{k+1} = W_k - \eta\frac{\frac{1-\mu}{1-\mu^{k+1}}\frac{\partial J}{\partial W_k} + \frac{\mu}{1-\mu^{k+2}}m_{k+1}}{\sqrt{\frac{n_{k+1}}{1-\nu^{k+1}}} + \varepsilon} \tag{11}$$

where μ and ν are hyperparameters controlling the moving average gradients and squared gradients, respectively. The hyperparameter ε serves to stabilize the learning rate and avoid zero division. The gradient of J with respect W_{ij} ($1 \le i \le N$, $1 \le j \le N$, $N = 2M$) is computed as:

$$\frac{\partial J}{\partial W_{ij}} = \frac{2}{L}\sum_{t=t_0}^{t_0+L}\sum_{k=1}^{M}(y_k(t) - \hat{y}_k(t))H_{ki}x_j(t-1)\Delta t \tag{12}$$

The whole optimization algorithm starts with initializing W (Fig. 1B). We will then randomly select an initial time t_0 and perform fixed-length Kalman Filter to estimate $x(t)$ based on W. Next, error gradient is calculated and W is updated according to NADAM. The updated W is then fed to the Kalman Filter to start off the next iteration until convergence.

2.5 Ground-truth Simulations

To evaluate the accuracy and efficiency of the LEMI framework, we generated 30 synthetic subjects by randomly selecting model parameters from uniform distribution: $W_{\text{RR}} \sim$ U(-0.02, 0.02), $W_{\text{EE}} \sim$ U(0.05, 0.2), $W_{\text{EI}} \sim$ U(0.05, 0.2), $W_{\text{IE}} \sim$ U(0.05, 0.5). We assumed W_{EI} to be fixed and set W_{II} to be zero as the effect of W_{EI} can be accounted by W_{IE} [18] and the I-I inhibition is much weaker than the I-E inhibition [22]. We randomly selected 10% inter-regional connections for sparse network construction. The ground-truth and composite neural activity was generated using Eqns. 1 - 3 with $\omega(t) \sim \mathcal{N}(0, 0.005)$ and $v(t) \sim \mathcal{N}(0, 0.01)$ and we simulated 9000 seconds of neural activity (TR = 1 sec). The composite neural activity was then convolved with a canonical hemodynamic response function (HRF) [8] to generate synthetic BOLD time series. We chose the canonical HRF due to its general applicability in fMRI modeling studies [13,24]. We run the LEMI for 20,000 iterations for good convergence and for each iteration, 20 temporal samples were selected (L = 20).

2.6 Empirical Dataset Application

After ground-truth validation, we applied the LEMI model to an empirical rs-fMRI dataset obtained from the ADNI database (`http://adni.loni.usc.edu/`). The dataset included 48 healthy normal control (NC) subjects (26/22 males/females, 73.4 $\pm$ 6.5 years), 48 subjects with MCI (31/17 males/females, 73.9 $\pm$ 10 years), and 48 patients with AD (27/21 males/females, 73.5 $\pm$ 8.5 years) who are age ($p = 0.95$, one-way ANOVA) and gender ($p = 0.55$, one-way ANOVA) matched. We used the fMRI dataset from a previous study where we selected the same number of age- and gender- matched NC and MCI subjects as AD subjects [18]. The 7-min fMRI data (TR = 3 sec) were processed with a standard pipeline [31] using AFNI [3]. Regional averaged BOLD rs-fMRI time series were extracted according to the Desikan-Killiany (DK) atlas [5] with 84 regions of interest (ROIs) including subcortical components. To reduce computational burden and focus on the networks that are most affected in AD [33], we selected 46 ROIs from the default mode (DMN), salience (SAL), frontoparietal control (FPC) and limbic (LIM) networks based on Yeo's seven network definition [32]. Structural connectivity (SC) was computed using probabilistic tractography based on the dMRI data consisting of 100 unrelated subjects from the WU-Minn Human Connectome Project (HCP) [7] because dMRI data was not available for all ADNI subjects. The dMRI data were preprocessed using the HCP protocol [15] and we conducted whole-brain tractography using asymmetry spectrum imaging (ASI) fiber tracking [30]. The SC matrix with 46 ROIs was extracted from the full SC matrix and averaged among the 100 subjects. We selected the strongest 10% SC connections for network modeling [18]; the results remained qualitatively similar with higher SC densities. For comparison, we applied regression DCM (rDCM) [13] to the ADNI data to estimate EC among 46 ROIs. We chose rDCM since it allows efficient estimation of whole-brain EC.

2.7 Statistical Analysis

We focused on E-I balance comparison among NC, MCI and AD subjects since studies suggest E-I imbalance plays an important role in AD pathophysiology [2,27]. For

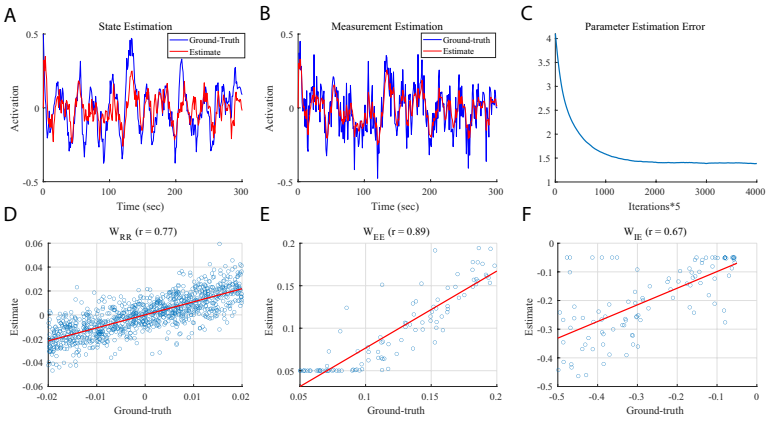

Fig. 2. Estimation results of one synthetic subject. (A) Estimation of E neural activity in one ROI using Kalman filter. (B) Prediction of deconvolved BOLD signal in one ROI. (C) Parameter estimation error computed as the norm of the difference between ground-truth parameters and estimated parameters. (D) Scatter plot of ground-truth W_{RR} and estimated W_{RR}. (E) Scatter plot of ground-truth W_{EE} and estimated W_{EE}. (F) Scatter plot of ground-truth W_{IE} and estimated W_{IE}.

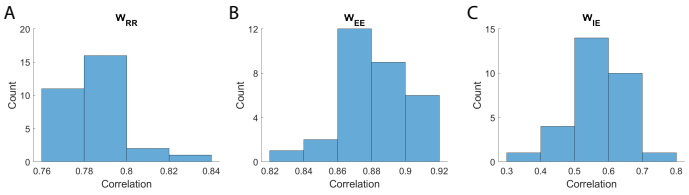

Fig. 3. Distribution of the correlation coefficients between estimated and ground-truth parameters for all 30 synthetic subjects. (A) Inter-regional W_{RR}. (B) Local recurrent excitation W_{EE}. (C) Local recurrent inhibition W_{IE}.

LEMI, we defined regional E-I balance as the ratio between recurrent excitation (W_{EE}) and recurrent inhibition (W_{IE}) strength in each ROI. For rDCM, the regional E-I balance is defined as the sum of all incoming EC (both excitatory and inhibitory) to a particular ROI as there is only one neural population per region in rDCM. One-way analysis of variance (ANOVA) was used to compare the E-I means of the three groups followed by post-hoc analysis with two-sample t-test. Multiple comparisons were corrected by controlling the false discovery rate (FDR) [1] with $q < 0.05$.

3 Results

3.1 Ground-truth Validation

The estimation results of one representative synthetic subject are shown in Fig. 2. The Kalman filter was able to accurately track the ground-truth neural activity (Fig. 2A)

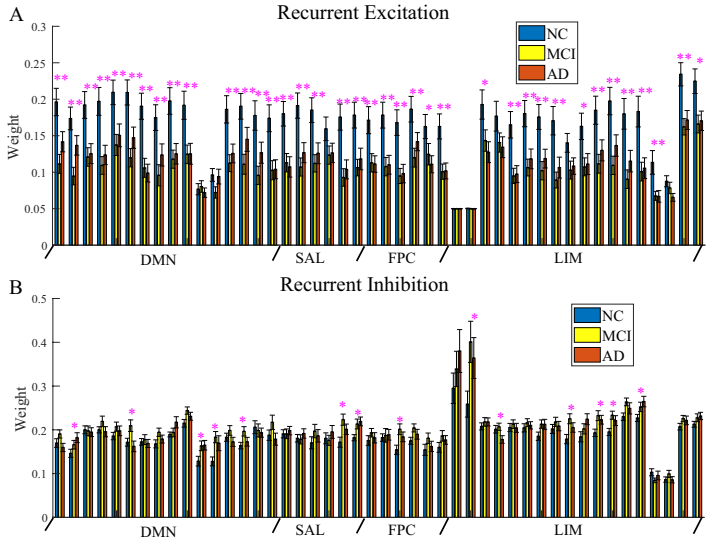

Fig. 4. Disrupted local excitation and inhibition in MCI and AD. (A) Comparison of recurrent excitation strength (W_{EE}) among NC, MCI and AD. (B) Comparison of recurrent inhibition strength (W_{IE}) among NC, MCI and AD. One star indicates uncorrected significance ($p < 0.05$) and double stars indicate significant group difference ($p < 0.05$; FDR corrected). DMN: default mode network; SAL: salience network; FPC: frontoparietal control network; LIM: limbic network.

and predict the deconvolved BOLD (Fig. 2B). The Root Mean Square Error (RMSE) of the neural state and measurement estimation was 0.15 ± 0.003 and 0.08 ± 0.0003, respectively. Also, the parameter estimation error rapidly converged to the minimum (Fig. 2C) and the computation time for a network with 100 regions took about 90 minutes (20,000 iterations) when run on a standard computer. The estimated connection parameters closely matched the ground-truth parameters ($r > 0.6$; Figs. 2D-F). The distribution of the correlation coefficients between estimated and ground-truth parameters for all 30 synthetic subjects is shown Fig. 3. Most of the correlation values were greater than 0.5 and the average correlation was 0.79 ± 0.01 for W_{RR}, 0.88 ± 0.02 for W_{EE} and 0.57 ± 0.08 for W_{IE}. The estimation results remained robust with higher measurement noise (R = 0.02) and different TR (TR = 2 or 3 sec). Overall, the simulation results demonstrate that LEMI can faithfully recover the ground-truth parameters.

3.2 Estimation of Empirical E-I Balance in AD

Application of the LEMI model to the ADNI dataset indicated that recurrent excitation (W_{EE}) in both MCI and AD was significantly decreased compared to NC ($p < 0.05$, FDR corrected) for most of the brain regions (Fig. 4A). In particular, one-way ANOVA showed significant group difference in 34 ROIs that passed FDR correction. In contrast, no significant difference in recurrent inhibition (W_{IE}) can survive multiple comparisons, though uncorrected significance showed a general trend of increased inhibition from

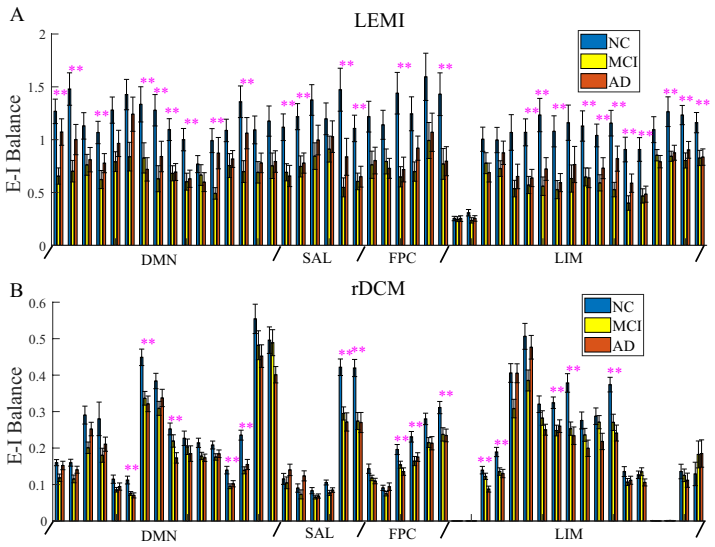

Fig. 5. Disrupted E-I balance in MCI and AD. (A) Comparison of LEMI-derived regional E-I balance among NC, MCI and AD. (B) Comparison of rDCM-derived regional E-I balance among NC, MCI and AD. Double stars indicate significant group difference ($p < 0.05$; FDR corrected).

NC to MCI/AD (Fig. 4B). Consequently, in more than half of ROIs (26), the regional E-I balance was significantly reduced in MCI/AD compared with NC ($p < 0.05$, FDR corrected; Fig. 5A). Consistently, the regional E-I balance estimated by rDCM was largely reduced in MCI/AD when compared with NC, but the degree of reduction was less prominent in rDCM and the number of regions that survived FDR correction was much lower (15 vs. 26) (compare Fig. 5B to Fig. 5A). This demonstrates that LEMI is more sensitive to detect E-I balance change in MCI/AD compared with rDCM by modeling intra-regional E-I interactions. Also, the widespread reduction in excitation is consistent with the disruption of synaptic transmission during AD progression [16], which can be utilized for early AD diagnosis.

4 Discussion and Conclusion

It should be recognized that to enable large-scale EC estimation, LEMI makes a number of simplifying assumptions including (1) the relative contribution of the excitatory and inhibitory neural activity to the deconvolved BOLD signal is 2:1; (2) the relationship between neural states and deconvolved BOLD is linear; and (3) the HRF is identical for all regions and subjects. Most of these assumptions are biologically plausible and have been made in previous studies [13,18,24], but their implications in EC estimation need to be fully investigated in future studies. In summary, we developed a new computational framework for large-scale EC estimation based on rs-fMRI and validated its efficiency and accuracy using both ground-truth simulation and empirical data. A

key advantage of LEMI lies in its enhanced biological realism by incorporating intra-regional E-I interactions, which allows more sensitive detection of neural circuit disruption in diseases. Overall, this framework offers a highly feasible yet biologically realistic method to construct brain-wide individualized EC network for disease diagnosis and the identification of circuit dysfunction in neurological and psychiatric disorders.

Acknowledgments. This study was supported in part by the United States National Institutes of Health (NIH) through grants R01MH125479, R01EB006733, R01EB008374, R01MH133836, and R01EB035160 to PTY, and R21AG083589 to GL.

Disclosure of Interests. The authors have no competing interests to declare that are relevant to the content of this article.

References

1. Benjamini, Y., Yekutieli, D.: The control of the false discovery rate in multiple testing under dependency. The Annals of Statistics **29** (8 2001). https://doi.org/10.1214/aos/1013699998
2. Busche, M.A., Konnerth, A.: Impairments of neural circuit function in alzheimer's disease. Philosophical Transactions of the Royal Society B: Biological Sciences **371**, 20150429 (8 2016). https://doi.org/10.1098/rstb.2015.0429
3. Cox, R.W.: AFNI: software for analysis and visualization of functional magnetic resonance neuroimages. Computers and biomedical research, an international journal **29**(3), 162–173 (Jun 1996). https://doi.org/10.1006/cbmr.1996.0014
4. Deco, G., Kringelbach, M.L.: Great expectations: using whole-brain computational connectomics for understanding neuropsychiatric disorders. Neuron **84**(5), 892–905 (Dec 2014). https://doi.org/10.1016/j.neuron.2014.08.034
5. Desikan, R.S., Ségonne, F., Fischl, B., Quinn, B.T., Dickerson, B.C., Blacker, D., Buckner, R.L., Dale, A.M., Maguire, R.P., Hyman, B.T., Albert, M.S., Killiany, R.J.: An automated labeling system for subdividing the human cerebral cortex on MRI scans into gyral based regions of interest. NeuroImage **31**(3), 968–980 (Jul 2006). https://doi.org/10.1016/j.neuroimage.2006.01.021
6. Dozat, T.: Incorporating Nesterov Momentum into Adam. In: Proceedings of the 4th International Conference on Learning Representations. pp. 1–4 (2016)
7. Essen, D.C.V., Smith, S.M., Barch, D.M., Behrens, T.E., Yacoub, E., Ugurbil, K.: The wu-minn human connectome project: An overview. NeuroImage **80**, 62–79 (10 2013). https://doi.org/10.1016/j.neuroimage.2013.05.041
8. Friston, K.J., Fletcher, P., Josephs, O., Holmes, A., Rugg, M.D., Turner, R.: Event-related fMRI: characterizing differential responses. NeuroImage **7**(1), 30–40 (Jan 1998). https://doi.org/10.1006/nimg.1997.0306
9. Friston, K.J., Harrison, L., Penny, W.: Dynamic causal modelling. NeuroImage **19**(4), 1273–1302 (Aug 2003). https://doi.org/10.1016/s1053-8119(03)00202-7
10. Friston, K.J., Preller, K.H., Mathys, C., Cagnan, H., Heinzle, J., Razi, A., Zeidman, P.: Dynamic causal modelling revisited. NeuroImage **199**, 730–744 (Oct 2019). https://doi.org/10.1016/j.neuroimage.2017.02.045
11. Friston, K., Moran, R., Seth, A.K.: Analysing connectivity with granger causality and dynamic causal modelling. Current Opinion in Neurobiology **23**, 172–178 (4 2013). https://doi.org/10.1016/j.conb.2012.11.010

12. Friston, K.J.: Functional and effective connectivity: a review. Brain connectivity **1**(1), 13–36 (2011). https://doi.org/10.1089/brain.2011.0008
13. Frässle, S., Harrison, S.J., Heinzle, J., Clementz, B.A., Tamminga, C.A., Sweeney, J.A., Gershon, E.S., Keshavan, M.S., Pearlson, G.D., Powers, A., Stephan, K.E.: Regression dynamic causal modeling for resting-state fmri. Human Brain Mapping **42**, 2159–2180 (5 2021). https://doi.org/10.1002/hbm.25357
14. Galán, R.F.: On how network architecture determines the dominant patterns of spontaneous neural activity. PLoS ONE **3**, e2148 (5 2008). https://doi.org/10.1371/journal.pone.0002148
15. Glasser, M.F., Sotiropoulos, S.N., Wilson, J.A., Coalson, T.S., Fischl, B., Andersson, J.L., Xu, J., Jbabdi, S., Webster, M., Polimeni, J.R., Essen, D.C.V., Jenkinson, M.: The minimal preprocessing pipelines for the human connectome project. NeuroImage **80**, 105–124 (10 2013). https://doi.org/10.1016/j.neuroimage.2013.04.127
16. Kashyap, G., Bapat, D., Das, D., Gowaikar, R., Amritkar, R.E., Rangarajan, G., Ravindranath, V., Ambika, G.: Synapse loss and progress of alzheimer's disease -A network model. Scientific reports **9**(1), 6555 (Apr 2019). https://doi.org/10.1038/s41598-019-43076-y
17. Kim, Y., Bang, H.: Introduction to Kalman Filter and Its Applications, chap. 2. IntechOpen (5 2018). https://doi.org/10.5772/intechopen.80600
18. Li, G., Hsu, L.M., Wu, Y., Bozoki, A.C., Shih, Y.Y.I., Yap, P.T.: Revealing excitation-inhibition imbalance in alzheimer's disease using multiscale neural model inversion of resting-state functional mri. Communications Medicine **5**, 17 (1 2025). https://doi.org/10.1038/s43856-025-00736-7
19. Li, G., Liu, Y., Zheng, Y., Wu, Y., Li, D., Liang, X., Chen, Y., Cui, Y., Yap, P.T., Qiu, S., Others: Multiscale neural modeling of resting-state fMRI reveals Executive-Limbic malfunction as a core mechanism in major depressive disorder. Neuroimage: Clinical **31**, 102758 (Jul 2021). https://doi.org/10.1016/j.nicl.2021.102758
20. Menon, V.: Large-scale brain networks and psychopathology: a unifying triple network model. Trends in cognitive sciences **15**(10), 483–506 (Oct 2011). https://doi.org/10.1016/j.tics.2011.08.003
21. Razi, A., Seghier, M.L., Zhou, Y., McColgan, P., Zeidman, P., Park, H.J., Sporns, O., Rees, G., Friston, K.J.: Large-scale DCMs for resting-state fMRI. Network neuroscience (Cambridge, Mass.) **1**(3), 222–241 (Oct 2017). https://doi.org/10.1162/NETN_a_00015
22. Riedemann, T.: Diversity and function of somatostatin-expressing interneurons in the cerebral cortex. International Journal of Molecular Sciences **20**, 2952 (6 2019). https://doi.org/10.3390/ijms20122952
23. Singh, M.F., Braver, T.S., Cole, M., Ching, S.: Precision data-driven modeling of cortical dynamics reveals person-specific mechanisms underpinning brain electrophysiology. Proceedings of the National Academy of Sciences **122** (1 2025). https://doi.org/10.1073/pnas.2409577121
24. Singh, M.F., Braver, T.S., Cole, M.W., Ching, S.: Estimation and validation of individualized dynamic brain models with resting state fMRI. NeuroImage **221**, 117046 (Nov 2020). https://doi.org/10.1016/j.neuroimage.2020
25. Sporns, O., Tononi, G., Kötter, R.: The human connectome: A structural description of the human brain. PLoS computational biology **1**(4), e42 (Sep 2005). https://doi.org/10.1371/journal.pcbi.0010042
26. Stephan, K., Iglesias, S., Heinzle, J., Diaconescu, A.: Translational perspectives for computational neuroimaging. Neuron **87**, 716–732 (8 2015). https://doi.org/10.1016/j.neuron.2015.07.008

27. Varela, E.V., Etter, G., Williams, S.: Excitatory-inhibitory imbalance in alzheimer's disease and therapeutic significance. Neurobiology of Disease **127**, 605–615 (7 2019). https://doi.org/10.1016/j.nbd.2019.04.010
28. Wiener, N.: Extrapolation, Interpolation, and Smoothing of Stationary Time Series. The MIT Press (3 1964). https://doi.org/https://doi.org/10.7551/mitpress/2946.001.0001
29. Wilson, H.R., Cowan, J.D.: Excitatory and inhibitory interactions in localized populations of model neurons. Biophysical Journal **12**, 1–24 (1 1972). https://doi.org/10.1016/S0006-3495(72)86068-5
30. Wu, Y., Hong, Y., Feng, Y., Shen, D., Yap, P.T.: Mitigating gyral bias in cortical tractography via asymmetric fiber orientation distributions. Medical Image Analysis **59**, 101543 (1 2020). https://doi.org/10.1016/j.media.2019.101543
31. Yan, C., Zang, Y.: DPARSF: a MATLAB toolbox for" pipeline" data analysis of resting-state fMRI. Frontiers in systems neuroscience **4**, 13 (2010). https://doi.org/10.3389/fnsys.2010.00013
32. Yeo, B.T.T., Krienen, F.M., Sepulcre, J., Sabuncu, M.R., Lashkari, D., Hollinshead, M., Roffman, J.L., Smoller, J.W., Zöllei, L., Polimeni, J.R., Fischl, B., Liu, H., Buckner, R.L.: The organization of the human cerebral cortex estimated by intrinsic functional connectivity. Journal of Neurophysiology **106**, 1125–1165 (9 2011). https://doi.org/10.1152/jn.00338.2011
33. Zott, B., Busche, M.A., Sperling, R.A., Konnerth, A.: What happens with the circuit in alzheimer's disease in mice and humans? Annual Review of Neuroscience **41**, 277–297 (7 2018). https://doi.org/10.1146/annurev-neuro-080317-061725